Article

SOURCE DATA | TRANSPARENT PROCESS

EMBO reports

FTO negatively regulates the cytotoxic activity of natural killer cells

Seok-Min Kim[1,2], Se-Chan Oh[1,2], Sun-Young Lee[1,3], Ling-Zu Kong[1,4], Jong-Hee Lee[2,5] & Tae-Don Kim[1,2,6,7,*]

Abstract

N^6-Methyladenosine (m^{6}A) is the most abundant epitranscriptomic mark and plays a fundamental role in almost every aspect of mRNA metabolism. Although m^{6}A writers and readers have been widely studied, the roles of m^{6}A erasers are not well-understood. Here, we investigate the role of FTO, one of the m^{6}A erasers, in natural killer (NK) cell immunity. We observe that FTO-deficient NK cells are hyperactivated. *Fto* knockout (*Fto*$^{-/-}$) mouse NK cells prevent melanoma metastasis *in vivo*, and FTO-deficient human NK cells enhance the antitumor response against leukemia *in vitro*. We find that FTO negatively regulates IL-2/15-driven JAK/STAT signaling by increasing the mRNA stability of suppressor of cytokine signaling protein (SOCS) family genes. Our results suggest that FTO is an essential modulator of NK cell immunity, providing a new immunotherapeutic strategy for allogeneic NK cell therapies.

Keywords epitranscriptome; FTO; m^{6}A regulator; N6-methyladenosine; NK cell

Subject Categories Cancer; Immunology; RNA Biology

DOI 10.15252/embr.202255681 | Received 29 June 2022 | Revised 21 December 2022 | Accepted 12 January 2023

EMBO Reports (2023) e55681

Introduction

In 1974, N^6-methyladenosine (m^{6}A) was first recognized as an abundant nucleotide modification in eukaryotic messenger RNA (mRNA; Desrosiers *et al*, 1974). m^{6}A methylation has fundamental roles in almost every aspect of mRNA metabolism, including mRNA stability and translation efficiency (Wang *et al*, 2014, 2015; Liu *et al*, 2015; Xiao *et al*, 2016; Roundtree *et al*, 2017; Li *et al*, 2017a), as well as in a variety of cellular processes (Fustin *et al*, 2013; Zhou *et al*, 2015; Ivanova *et al*, 2017; Kan *et al*, 2017; Xiang *et al*, 2017). Consistent with these critical roles, aberrant m^{6}A methylation has affected numerous cellular processes, resulting in tumorigenesis and tumor progression (Zhang *et al*, 2016; Kwok *et al*, 2017; Chen *et al*, 2018). The m^{6}A regulators include "writers" and "erasers," which add and remove methylation marks, respectively, and "readers," which recognize and bind to these marks (Niu *et al*, 2013). As m^{6}A levels are highly stable throughout the mRNA life cycle, dynamic m^{6}A erasers may be limited to specific conditions (Darnell *et al*, 2018). Therefore, most research has focused on writers and readers. However, recent studies have demonstrated that cross-talk between writers, readers, and erasers is essential for cancer growth and progression (Panneerdoss *et al*, 2018) and have revealed the importance of m^{6}A dynamics, rather than total level (Zhang *et al*, 2020), (Yang *et al*, 2021). These findings emphasize the need for further studies of erasers (Shulman & Stern-Ginossar, 2020).

The fat mass and obesity-associated (FTO) protein are one of the m^{6}A erasers. In 2011, FTO was identified as the first demethylase of m^{6}A residues in single-stranded RNA (Jia *et al*, 2011). FTO plays a vital role in tumorigenesis in various cancer types, such as acute myeloid leukemia (Huang *et al*, 2019), and breast cancer (Niu *et al*, 2019), and in cancer stem cells (Su *et al*, 2020); however, few studies have evaluated its roles in immune cells (Gu *et al*, 2020).

m^{6}A methylation is involved in almost all immune cells, such as dendritic cells (Han *et al*, 2019; Wang *et al*, 2019; Liu *et al*, 2019a), macrophages (Yu *et al*, 2019; Liu *et al*, 2019b; Tong *et al*, 2021), T cells (Li & Rudensky, 2016; Li *et al*, 2017b; Furlan *et al*, 2019; Zhu *et al*, 2019), B cells (Zheng *et al*, 2020; Huang *et al*, 2022), and hematopoietic stem cells (Zhang *et al*, 2017; Li *et al*, 2018; Lv *et al*, 2018; Cheng *et al*, 2019; Lee *et al*, 2019; Yin *et al*, 2022). As such, there have been many reports on the functional role of m^{6}A in immune cells, but few studies using m^{6}A eraser (Gu *et al*, 2020; Zhou *et al*, 2021; Ding *et al*, 2022). Although recently reported for m^{6}A in NK cells (Ma *et al*, 2021; Song *et al*, 2021), it is less well-known compared with other immune cells. NK cells are large granular lymphoid cells with a crucial role in innate immune responses against virus/pathogen-infected cells and transformed cells (Vivier *et al*, 2008). IL-2 and IL-15 are essential for NK cell function and have

1 Immunotherapy Research Center, Korea Research Institute of Bioscience and Biotechnology (KRIBB), Daejeon, Korea
2 Department of Functional Genomics, KRIBB School of Bioscience, Korea University of Science and Technology (UST), Daejeon, Korea
3 Division of Life Science, Korea University, Seoul, Korea
4 Department of Biochemistry, Chungnam National University, Daejeon, Korea
5 National Primate Research Center (NPRC), KRIBB, Cheongju, Korea
6 Biomedical Mathematics Group, Institute for Basic Science (IBS), Daejeon, Korea
7 Department of Biopharmaceutical Convergence, School of Pharmacy, Sungkyunkwan University, Suwon, Korea
*Corresponding author. Tel: +82 42 860 4236; E-mail: tdkim@kribb.re.kr

© 2023 The Authors

14693178, 0, Downloaded from https://www.embopress.org/doi/10.15252/embr.202255681 by Korea Research Institute Of, Wiley Online Library on [06/03/2023]. See the Terms and Conditions (https://onlinelibrary.wiley.com/terms-and-conditions) on Wiley Online Library for rules of use; OA articles are governed by the applicable Creative Commons License

been used as immunotherapeutic agents to promote NK cell antitumor activity (Becknell & Caligiuri, 2005). Suppressor of cytokine signaling proteins (SOCS; CISH, SOCS1-7) is a negative regulator that inhibit IL-2/15 signaling in a negative feedback loop (Hilton *et al*, 1998). Among SOCS family genes, SOCS3 inhibits the anticancer efficacy of human primary NK cells (Naeimi Kararoudi *et al*, 2018).

Here, we investigated the role of the FTO in NK cell immunity. We evaluated tumor-killing activity, pro-inflammatory cytokine production, cell viability, and activating receptor expression in Fto-deficient NK cells, as well as downstream effects on melanoma metastasis and antitumor response to leukemia cells. We further studied the effect of FTO on mRNA stability and IL-2/15-driven JAK/STAT signaling. Our results suggest that FTO is an essential modulator of cytokine-induced NK cell activation, providing a potential new allogeneic NK cell therapy to increase cytokine sensitivity by blocking FTO function.

Results

Fto$^{-/-}$ mice are resistant to experimental tumor metastasis due to enhanced splenic NK cell activity

To investigate the physiological role of Fto in NK cells, we generated mice with a germline *Fto* deletion (*Fto*$^{-/-}$) by using the CRISPR/Cas9 system (pT7 plasmid) to induce a deletion in the first exon with the start codon (Fig EV1A–C). We confirmed the absence of Fto protein expression in various mouse tissues and detected higher m^{6}A levels in the spleen and bone marrow in *Fto*$^{-/-}$ mice than in wild-type mice (*Fto*$^{+/+}$; Figs EV1D and 1A). As already reported, Fto protein expression is elevated in tissues of the lymphatic system, such as the spleen (Fan *et al*, 2015). *Fto*$^{-/-}$ mice were healthy; however, consistent with previous results, their body weights were slightly lower than those of *Fto*$^{+/+}$ mice (Fischer *et al*, 2009). Populations of CD3$^-$NK1.1$^+$ NK cells in the spleen, blood, and bone marrow were similar in *Fto*$^{-/-}$ mice and *Fto*$^{+/+}$ mice (Fig EV1E).

One of the syngeneic mouse tumor cell lines known to activate and be controlled by NK cells, B16F10, was injected into *Fto*$^{+/+}$ and *Fto*$^{-/-}$ mice. The intravenous (*i.v.*) administration of B16F10 melanoma cells to *Fto*$^{+/+}$ mice resulted in extensive metastatic nodule formation in the lung after 14 days. By contrast, B16F10 metastatic nodules were largely absent from *Fto*$^{-/-}$ mice (Fig 1B). Interferon-gamma (Ifng) levels in the blood were higher in *Fto*$^{-/-}$ mice than in *Fto*$^{+/+}$ mice after intravenous injection of B16F10 melanoma cells (Fig EV2A). This finding was consistent with the prolonged survival after intravenous injection of EL4 lymphoma cells into *Fto*$^{+/+}$ and *Fto*$^{-/-}$ mice (Fig 1C). *Fto*$^{-/-}$ mice showed significantly longer survival times than those of *Fto*$^{+/+}$ mice. In addition, in the B16F10 xenograft mouse model, the growth of tumors was decreased in *Fto*$^{-/-}$ mice than in *Fto*$^{+/+}$ mice (Fig 1D and E).

To confirm that the reduced B16F10 metastatic nodule formation observed in *Fto*$^{-/-}$ mice was due to enhanced NK cell activity, we treated *Fto*$^{+/+}$ and *Fto*$^{-/-}$ mice with an anti-NK1.1 antibody to deplete NK cells. The depletion of NK cells in *Fto*$^{-/-}$ mice resulted in similar B16F10 metastatic nodule formation to that of *Fto*$^{+/+}$ mice (Figs 1F and EV2B). These results suggest that Fto specifically functions in NK cells in the B16F10 metastasis mouse model. Furthermore, after the *ex vivo* activation of NK cells for 24 or 48 h with IL-2 and IL-15, *Fto*$^{-/-}$ splenic NK cells showed significantly greater ($P < 0.05$) cytotoxicity against EL4 lymphoma (Fig 1G) and YAC1 lymphoma (Fig EV2C) than that of *Fto*$^{+/+}$ splenic NK cells. The hyperactivity of *Fto*$^{-/-}$ splenic NK cells also resulted in higher levels of IL-2/15-derived Ifng production than those for *Fto*$^{+/+}$ splenic NK cells after *ex vivo* activation for 24 h (Fig 1H, left). In addition, *Ifng* mRNA levels were higher in *Fto*$^{-/-}$ splenic NK cells than in *Fto*$^{+/+}$ splenic NK cells (Fig 1H, right). Altogether, these results indicated that Fto acts as a negative regulator in NK cell activity.

FTO-deficient NK92 cells are hyperactivated

To gain insight into the molecular mechanism underlying m^{6}A and FTO-dependent regulation in NK cells, we transiently reduced the expression of FTO in the NK92 cell line (NK92-siFTO) using small interfering RNA (siRNA). NK92 is widely used for NK cell experiments. After FTO expression was decreased by using siRNA, m^{6}A levels were higher than those in control siRNA-transfected NK92 cells (NK92-siCTRL; Fig 2A). After co-culture with K562 cells for 4 h, NK92-siFTO cells displayed greater ($P < 0.01$) cytotoxicity (Fig 2B) and degranulation activity (Fig 2C) at various ratios of NK92: K562 cells than those of NK92-siCTRL cells. And protein expression of Granzyme B (GZMB) was greater in NK92-siFTO cells than in NK92-siCTRL cells after IL-2 treatment (Fig 2D). Moreover, the release of cytokines (IFNγ and tumor necrosis factor-α, TNFα) from NK92-siFTO cells was elevated after IL-2 treatment for 24 h or after co-culture with K562 cells for 4 h (Fig 2E). These increased cytokine levels may support the enhanced NK cell-mediated cancer cell-killing activity. Additionally, the opposite results were obtained after FTO was overexpressed (NK92 + MOCK, NK92 + FTO; Fig EV3A–C). The effects were similar to those observed after the overexpression of METTL3 (NK92 + MOCK, NK92 + METTL3; Fig EV3D–F). In addition to the enhancement of NK cell activity, cell viability after co-culture with or without K562 cells, and mRNA expression levels of the anti-apoptotic factors, *BCL2*, *BCL-XL*, and *PIM1*, after IL-2 treatment were higher in NK92-siFTO cells than in NK92-siCTRL cells (Fig EV4A and B). Next, we checked the cell surface expression of the activating receptors (NKG2D, NKp30, NKp44, NKp46, and CD16), IL-2 receptor α (CD25), TNF receptor (CD27), and TGFβ receptor (CD105) in NK92 cells. Inhibitory receptors are rarely expressed in the NK92 cell line. NK92-siFTO cells displayed slightly higher levels of only NKp30 than those in NK92-siCTRL cells (Fig EV4C). This difference was heightened after culture in IL-2 (Fig EV4D). Overall, the killing activity, cytokine production, and cell viability were improved, and the expression levels of activating receptors, especially NKp30, were slightly higher in NK92-siFTO cells than in NK92-siCTRL cells. Altogether, these results indicated that FTO-deficient NK92 cell activity was greater than that of wild-type NK92 cells.

FTO affects JAK/STAT signaling levels

FTO-deficient NK cells (*Fto*$^{-/-}$ splenic NK cells and NK92-siFTO) exhibited greater anti-cancer effects than those of wild-type NK cells (*Fto*$^{+/+}$ splenic NK cells and NK92-siCTRL; Figs 1 and 2). To understand the biological mechanisms underlying the enhanced cytotoxicity, cytokine release, and cell viability, we investigated signaling pathways in NK cells. Cytokine signaling pathways are essential for

© 2023 The Authors

14693178, 0, Downloaded from https://www.embopress.org/doi/10.15252/embr.202255681 by Korea Research Institute Of, Wiley Online Library on [06/03/2023]. See the Terms and Conditions (https://onlinelibrary.wiley.com/terms-and-conditions) on Wiley Online Library for rules of use; OA articles are governed by the applicable Creative Commons License

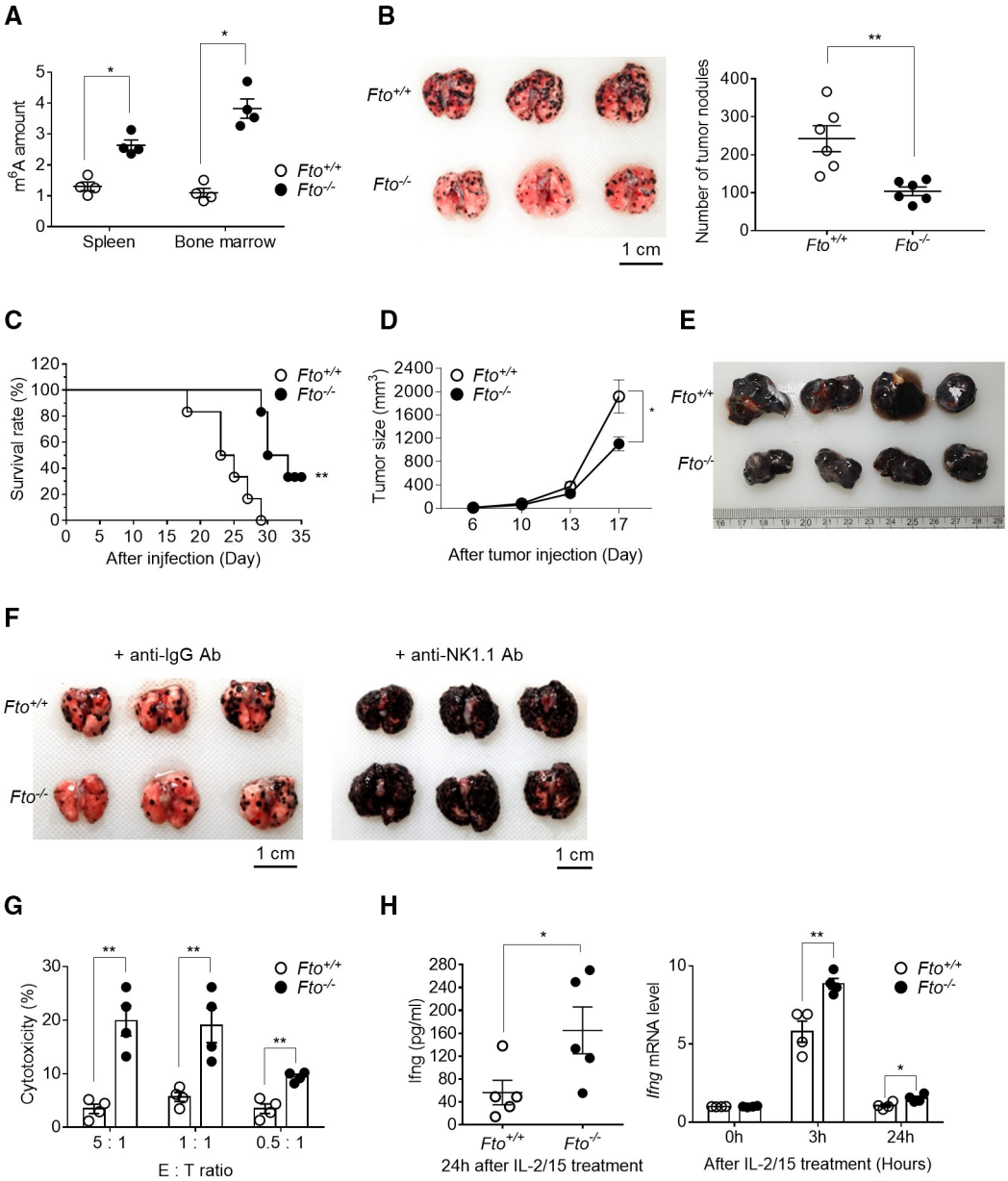

Figure 1. Loss of Fto expression enhances the anti-metastatic activity of mouse NK cells isolated from the spleen.

A m^{6}A levels in total RNA from the spleen and bone marrow of *Fto*$^{+/+}$ or *Fto*$^{-/-}$ mice were measured by ELISA (n = 4/group).

B Image of the lung surface (left) and numbers of metastatic nodules (right) 14 days following the injection of B16F10 melanoma cells (n = 8/group).

C Survival curves after the injection of EL4 lymphoma cells (n = 6/group).

D, E Tumor volume (D) and image of the tumor (E) 17 days following the subcutaneous injection (*s.c.*) of B16F10 melanoma cells (n = 4/group). Tumor size was calculated using the formula length × width^2 × 0.5.

F Metastatic burden in the lung after treatment with an IgG control antibody (anti-IgG Ab) or anti-NK1.1 antibody for NK cell depletion on days −4, −1, and 2 relatives to B16F10 cell injection (n = 3/group).

G EL4 cell-killing activity by NK cells isolated from the spleen was measured by calcein AM-based assays at the indicated NK:EL4 (E:T, n = 4/group).

H Ifng protein and *Ifng* mRNA levels (n = 4/group) were determined by ELISA and quantitative PCR.

Data information: Error bars represent s.e.m. Significance was determined using the Mann–Whitney *U* (A, B), Mantel–Cox (C), two-way ANOVA (D), or Student's *t*-tests (G, H): $^{**}P < 0.01$; $^{*}P < 0.05$.
Source data are available online for this figure.

NK cells, which are mainly primed by the IL-2, IL-15, and JAK/STAT signaling cascade (Becknell & Caligiuri, 2005). Therefore, we predicted that m^{6}A RNA methylation affects the IL-2/15 signaling pathway. In NK92-siFTO cells, levels of IL-2-stimulated JAK1 and JAK3 phosphorylation were higher than those in NK92-siCTRL. It was coupled with extended phosphorylation kinetics (Fig 3A).

© 2023 The Authors

14693178, 0, Downloaded from https://www.embopress.org/doi/10.15252/embr.202255681 by Korea Research Institute Of, Wiley Online Library on [06/03/2023]. See the Terms and Conditions (https://onlinelibrary.wiley.com/terms-and-conditions) on Wiley Online Library for rules of use; OA articles are governed by the applicable Creative Commons License

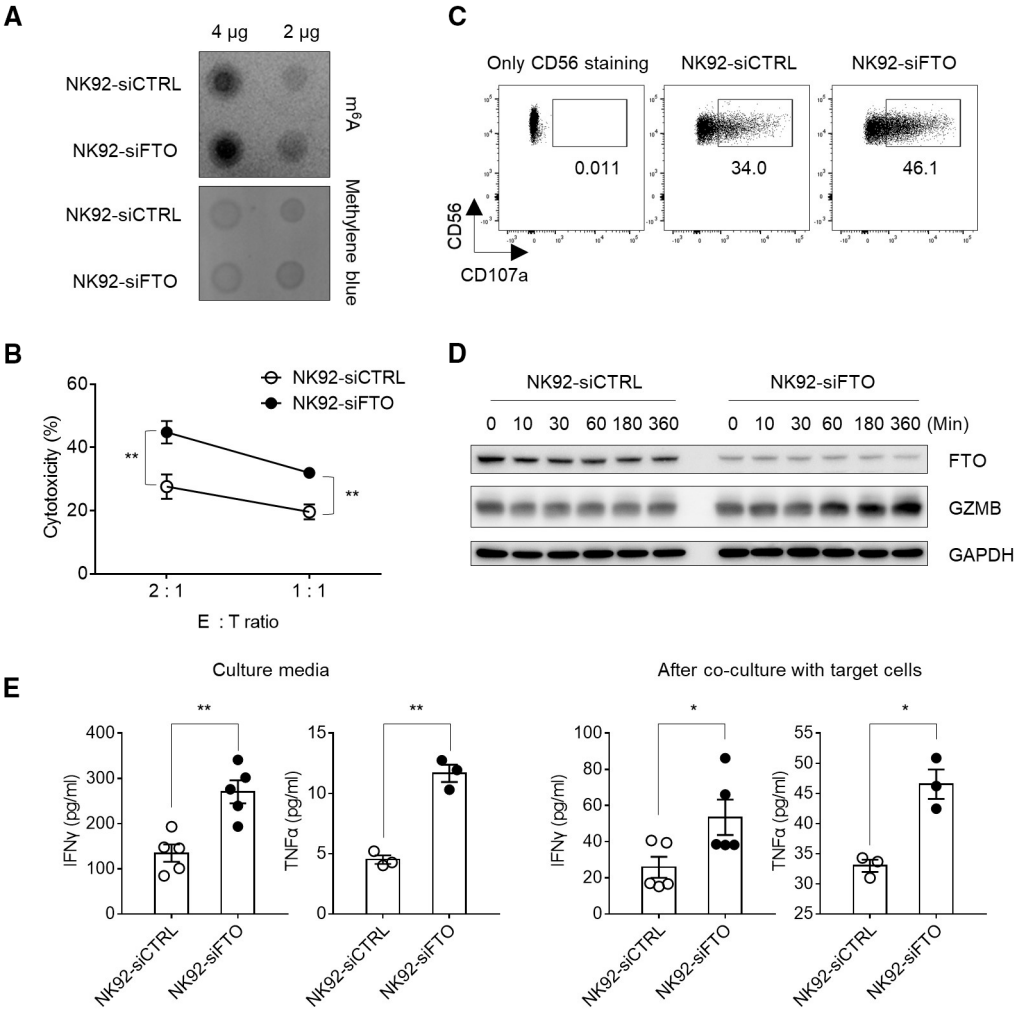

Figure 2. FTO-deficient NK92 cells display superior killing effects and high cytokine production.

A m^6A dot blot assay using total RNA from NK92-siCTRL or NK92-siFTO cells.

B K562 leukemia cell-killing activity by NK92-siCTRL or NK92-siFTO cells was measured by a calcein AM-based cytotoxicity assay at the indicated NK92:K562 (E:T, effector:target) ratio ($n = 6$ biological replicates).

C Degranulation was measured by flow cytometry. Values indicate percentages.

D Western blotting for the detection of GZMB in NK92-siCTRL and NK92-siFTO cells after treatment with IL-2.

E Levels of IFNγ ($n = 5$ biological replicates) and TNFα ($n = 3$ biological replicates) in the culture media 24 h after IL-2 treatment (left) or co-culture media with K562 cells for 4 h (right) were determined by ELISA.

Data information: Error bars for panels (B and E) are ± s.e.m. For panels (A, C, and D), data are representative of two (C, D) or three times (A) independent experiments with similar results. Significance was determined using the Mann–Whitney *U* test (B) or Student's *t*-tests (E): $^{**}P < 0.01$; $^{*}P < 0.05$.
Source data are available online for this figure.

Additionally, total JAK1 and JAK3 levels were higher in NK92-siFTO cells, as evident in resting cells before IL-2 stimulation (Fig 3A, 0 h). The mRNA expression levels of the JAK/STAT target genes (*GZMB*, *TNFα*, and *MYC*) were also increased (Appendix Fig S1). Similarly, in cells expanded in IL-2, we observed higher basal expression levels of JAK3, STAT3, and phosphorylated STAT3 and STAT5 after the withdrawal of IL-2 (Fig 3B). Alternatively, when FTO was overexpressed, the phosphorylation levels of JAK1 and JAK3 were lower than those in NK92 + MOCK cells following activation by IL-2 (Fig 3C). Thus, these results demonstrated that FTO regulates IL-2-induced JAK/STAT signaling pathways.

FTO regulates mRNA stability of SOCS family genes by the demethylation of m^6A

Interestingly, the mRNA expression of the SOCS family genes, especially *SOCS3*, was significantly lower ($P < 0.001$) in NK92-siFTO cells than in NK92-siCTRL cells before IL-2 activation (Fig 4A), resting $Fto^{-/-}$ mouse splenic NK cells and whole spleen cells (Fig EV5A and B). The SOCS family genes are critical negative regulators that inhibit cytokine signaling in a negative feedback loop (Hilton *et al*, 1998). They consist of a central SH2 domain, which binds to a phosphorylated tyrosine residue in target proteins and a C-terminal

© 2023 The Authors

14693178, 0, Downloaded from https://www.embopress.org/doi/10.15252/embr.202255681 by Korea Research Institute Of, Wiley Online Library on [06/03/2023]. See the Terms and Conditions (https://onlinelibrary.wiley.com/terms-and-conditions) on Wiley Online Library for rules of use; OA articles are governed by the applicable Creative Commons License

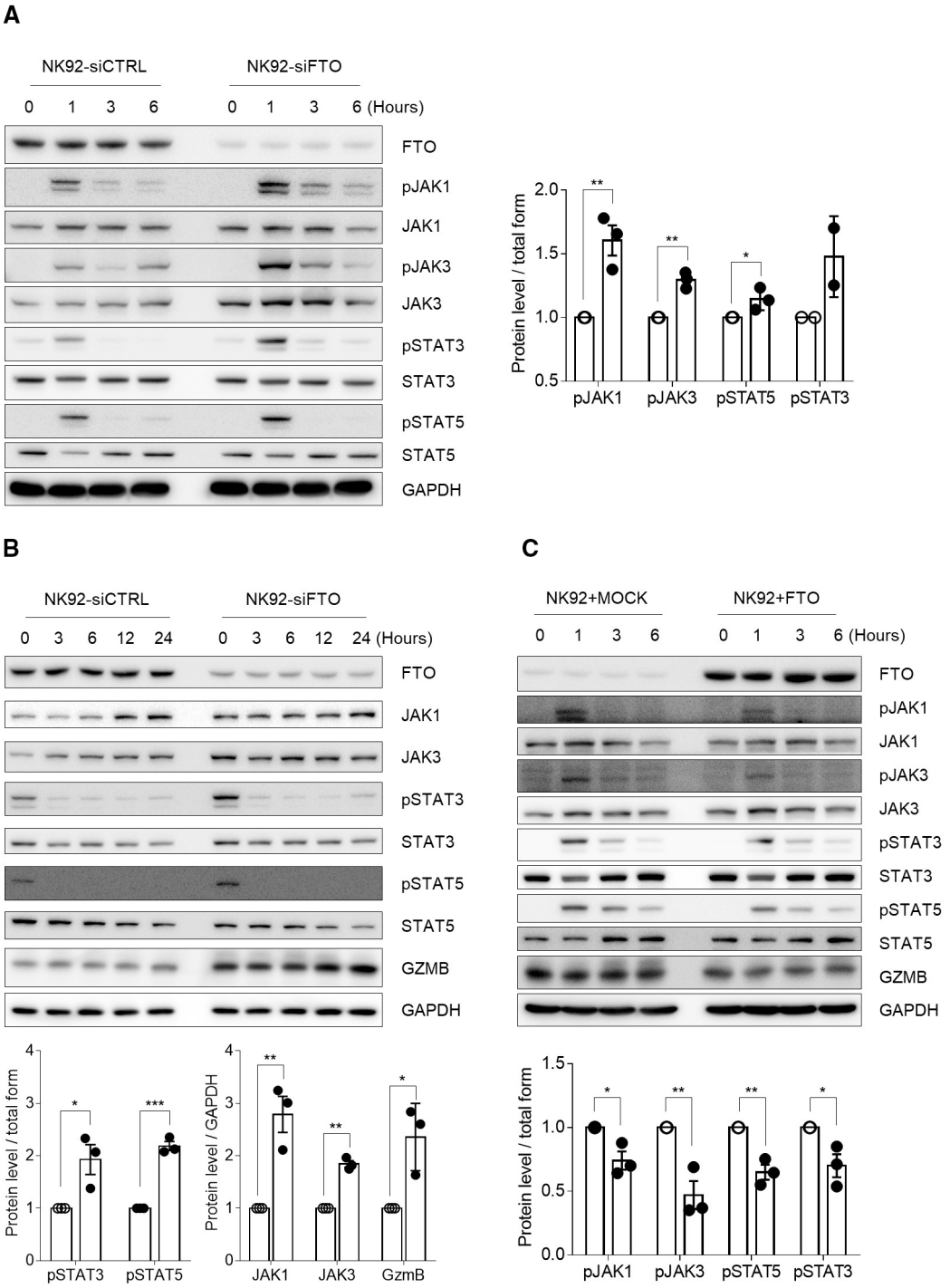

Figure 3. FTO regulates the JAK/STAT signaling pathway.

A Western blotting analysis of NK92-siCTRL and NK92-siFTO cells incubated with 20 ng/ml IL-2 for the indicated times was performed. Cells were lysed and analyzed by immunoblotting with antibodies to the indicated phosphorylated (p) and total proteins ($n = 2 \sim 3$).

B Western blotting analysis. NK92-siCTRL or NK92-siFTO cells were incubated with 20 ng/ml IL-2 for 24 h, washed, and cultured without IL-2 (IL-2 depletion) for the indicated times ($n = 3$).

C A western blotting analysis of NK92 + MOCK or NK92 + FTO cells incubated with 20 ng/ml IL-2 for the indicated times was performed ($n = 3$).

Data information: Western blotting data are representative of at least two times independent experiments with similar results. The protein levels were expressed as the relative band density of the corresponding protein (A is on the right, and B and C are on the lower). Error bars are ± s.e.m. Significance was determined using the Student's *t*-tests: ***$P < 0.001$; **$P < 0.01$; *$P < 0.05$.
Source data are available online for this figure.

© 2023 The Authors

14693178, 0, Downloaded from https://www.embopress.org/doi/10.15252/embr.202255681 by Korea Research Institute Of, Wiley Online Library on [06/03/2023]. See the Terms and Conditions (https://onlinelibrary.wiley.com/terms-and-conditions) on Wiley Online Library for rules of use; OA articles are governed by the applicable Creative Commons License

SOCS box domain (Krebs & Hilton, 2001). The SOCS box domain recruits the E3 ubiquitin ligase complex that ubiquitinates target proteins, inducing proteasomal degradation. In addition, SOCS1 and SOCS3 bind directly to JAK1, JAK2, and tyrosine kinase 2 (TYK2), inhibiting JAK enzymatic activity via the KIR domain (Baker *et al*, 2009). The rate of proliferation and cytotoxicity are elevated in *SOCS3*-deleted human NK cells (Naeimi Kararoudi *et al*, 2018), suggesting that SOCS3 can be used in NK cell-based immunotherapy (Gotthardt *et al*, 2019). To explore the mechanism underlying the regulatory effects of FTO on SOCS3 expression, we further validated the expression patterns of SOCS family genes by western blotting (Figs 4B and EV5C). The protein expression levels of CISH, SOCS1, and SOCS3 were decreased, with significantly lower SOCS3 expression in NK92-siFTO cells than in NK2-siCTRL cells. Moreover, we confirmed that the protein level of SOCS3 was changed according to the expression of FTO or METTL3 (Fig EV5D and E), and the mRNA expression pattern of *SOCS3* differs according to the IL-2 treatment (Fig EV5F). The mRNA level of *SOCS3* was higher in NK92 + METTL3 cells than in NK92 + MOCK cells 24 h after IL-2 treatment (Fig EV5F, left). Conversely, after 24 h of IL-2 depletion, *SOCS3* mRNA levels were decreased in NK92 + METTL3 cells but increased in NK92 + FTO cells compared with levels in NK92 + MOCK cells (Fig EV5F, right). These results indicate that *SOCS3* is a target gene of JAK/STAT signaling and that *SOCS3* expression is precisely regulated by the m^{6}A regulators FTO and METTL3. Next, we performed m^{6}A-specific immunoprecipitation (MeRIP) and quantitative PCR (qPCR) assay to check the m^{6}A status in NK cells. In NK92-siFTO cells, the total mRNA levels (input) of *SOCS1* and three were decreased, but the levels of the m^{6}A methylated mRNA (MeRIP) were increased (Fig 4C, upper panel). The opposite results were obtained in NK92 + FTO cells (Fig 4C, lower panel), suggesting that m^{6}A was present in the mRNA of the SOCS family genes and can be regulated by FTO. Additionally, using the 3'UTR reporter system confirmed that m^{6}A exists in the 3'UTR of *SOCS3* and *CISH*, regulated by FTO (Figs 4D and EV5G). Altogether, these results indicated that FTO influences the intensity of JAK/STAT signaling by modulating the stability of *SOCS3* mRNA through demethylation.

FTO-deficient CD3$^-$CD56$^+$ human NK cells derived from umbilical cord blood showed enhanced activity

To extend the results to human primary NK cells, we used human primary CD3$^-$CD56$^+$ NK cells derived from umbilical cord blood (UCB). Similar to the experiment using the NK92 cell line, we transiently reduced the expression of FTO in the human primary NK cells (CD56$^+$-siFTO). After FTO expression was decreased by using siRNA, CD56$^+$-siFTO cells displayed significantly enhanced killing activity at various effector:target cell ratios compared to that of control siRNA-transfected CD56$^+$ cells (CD56$^+$-siCTRL; Fig 5A). Similarly, the mRNA expression levels of cytokine and effector molecules, *IFNγ*, *GZMB*, and perforin 1 (*PRF1*), increased more substantially ($P < 0.05$) in the CD56$^+$-siFTO cells than in CD56$^+$-siCTRL cells (Fig 5B). Western blotting showed that the strength of cytokine-stimulated phosphorylation of JAK1 and STAT3 was greater in the CD56$^+$-siFTO cells than in CD56$^+$-siCTRL cells after cytokine treatment (Fig 5C). Moreover, the protein expression levels of CISH, SOCS1, and SOCS3 were decreased in CD56$^+$-siFTO cells (Fig 5D). Therefore, these results showed that FTO also plays a negative regulatory role in human primary CD3$^-$CD56$^+$ NK cells.

FTO-deficient NK92 cells enhance the antitumor responses against K562 leukemia

Allogeneic NK cell therapy is a potential therapeutic strategy for a variety of cancers. Adoptive cell transfer (ACT) is one of the main branches of cancer immunotherapy and has promising clinical benefits (Lupo & Matosevic, 2019). Unlike T cell therapy, NK cell therapy can be used for allogeneic, off-the-shelf treatment. It has fewer side effects, such as graft-versus-host disease (GvHD) or cytokine storm syndrome (Bald *et al*, 2020). Owing to these advantages, NK cell therapy has been used broadly as an immunotherapeutic strategy. To exploit the potential clinical application of FTO in NK cells, we produced NK92 cells (NK92-shFTO) with permanent FTO knockdown by lentiviral infection (Fig 6A). Similar to the results of NK92 cells (NK92-siFTO) with transient FTO knockdown, NK92-shFTO cells exerted a higher killing effect ($P < 0.01$) and degranulation activity ($P < 0.001$) against luciferase-expressing K562 cells (K562-Luc) or normal K562 cells than those of NK92-TRC control cells (Fig 6B and C, and Appendix Fig S2A and B). After IL-2 activation, levels of IL-2 stimulated phosphorylation of JAK1 and JAK3 were higher and protein expression levels of CISH, SOCS1, and SOCS3 were lower in NK92-shFTO cells than in NK92-TRC cells (Appendix Fig S2C). The mRNA expression levels of *IFNγ*, *GZMB*, *BCL-XL*, and *PIM1* were also higher in NK92-shFTO cells than in NK92-TRC cells (Appendix Fig S2D).

To test whether NK92-shFTO affects tumor-killing during ACT, we injected K562-Luc cells at day 0. Moreover, NK92-TRC or NK92-shFTO were transfused three times into NOD.Cg-Prkdcscid Il2rgtm1Sug/Jic (NSG) mice intravenously (Fig 6D). Interestingly, mice injected with NK92-shFTO cells had significantly weaker bioluminescence signals and higher survival rates than those of mice injected with NK92-TRC cells (Fig 6E–G). Therefore, NK92-shFTO cells enhanced the antitumor responses against K562 leukemia. These findings suggest that FTO may be a new immunotherapeutic strategy in allogeneic NK cell therapy.

Discussion

FTO is one of the m^{6}A erasers. Several independent genome-wide association studies have revealed that FTO is associated with obesity and type 2 diabetes in humans (Dina *et al*, 2007; Hinney *et al*, 2007; Scuteri *et al*, 2007; Samaan *et al*, 2013). Subsequent studies in mice have demonstrated that FTO expression levels affect the body mass index (Fischer *et al*, 2009). Single nucleotide polymorphism (SNP) in the first intron of *FTO* is functionally connected to and directly interacts with the promoters of *IRX3*, increasing the expression of IRX3 (Smemo *et al*, 2014). However, there is no direct relationship between FTO protein expression and obesity. In 2011, FTO was identified as the first demethylase of m^{6}A residues in single-stranded RNA; furthermore, the demethylation activity of FTO was related to adipogenesis (Jia *et al*, 2011; Zhao *et al*, 2014). In addition, FTO has established roles in cancer (Huang *et al*, 2019; Niu *et al*, 2019; Su *et al*, 2020), cardiac function (Mathiyalagan *et al*, 2019), and hippocampal memory formation (Walters

© 2023 The Authors

14693178, 0, Downloaded from https://www.embopress.org/doi/10.15252/embr.202255681 by Korea Research Institute Of, Wiley Online Library on [06/03/2023]. See the Terms and Conditions (https://onlinelibrary.wiley.com/terms-and-conditions) on Wiley Online Library for rules of use; OA articles are governed by the applicable Creative Commons License

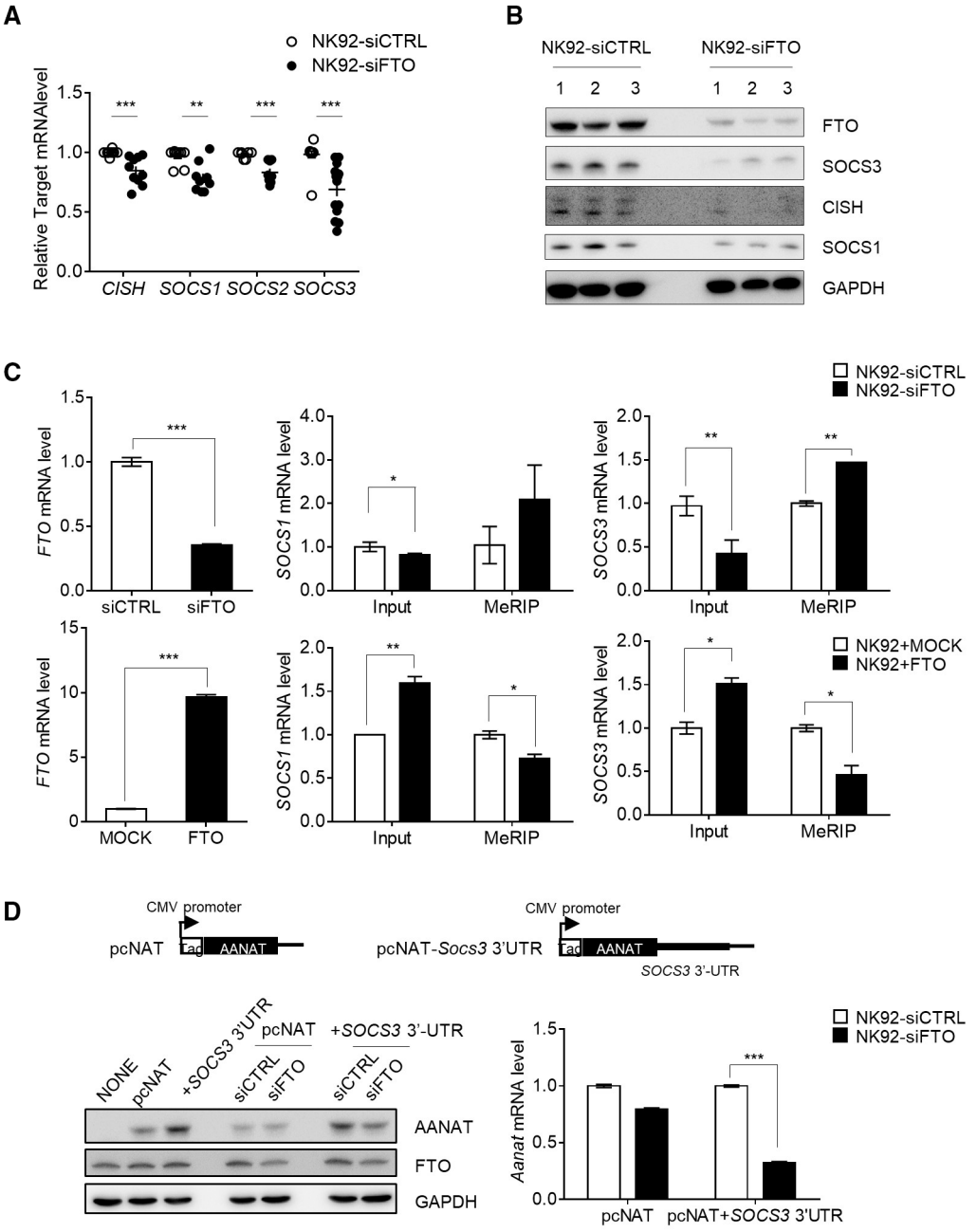

Figure 4. FTO controls mRNA stability of SOCS family members by removing m^{6}A RNA modifications.

A Relative mRNA expression levels of SOCS family proteins were determined by qPCR after cultivation without IL-2 for 24 h ($n > 8$ biological replicates).

B Western blotting analysis of SOCS3, CISH, and SOCS1 in NK92-siCTRL or NK92-siFTO cells ($n = 3$ biological replicates).

C m^{6}A methylated RNA immunoprecipitation and quantitative PCR (MeRIP-qPCR) analysis using a m^{6}A antibody in NK92-siFTO (upper) or NK92 + FTO (lower) cells compared with NK92-siCTRL or NK92 + MOCK cells.

D *SOCS3* 3'-UTR reporter assay using the AANAT reporter system. Plasmid information for the AANAT reporter system with or without the *SOCS3* 3'-UTR sequence (upper). Levels of Aanat protein (left) and *Aanat* mRNA (right) expression in HEK-293T cells co-transfected with plasmid-expressing AANAT reporter containing *SOCS3* 3'-UTR and siCTRL or siFTO.

Data information: Error bars for panel (A) are ± s.e.m. Error bars for panels (C and D) are ± s.d. based on technical triplicates. For panels (C and D), data are representative of three times independent experiments with similar results. Significance was determined using the Mann–Whitney *U* test (A) or Student's *t*-tests (C, D): ***$P < 0.001$; **$P < 0.01$; *$P < 0.05$.

Source data are available online for this figure.

© 2023 The Authors

14693178, 0, Downloaded from https://www.embopress.org/doi/10.15252/embr.202255681 by Korea Research Institute Of, Wiley Online Library on [06/03/2023]. See the Terms and Conditions (https://onlinelibrary.wiley.com/terms-and-conditions) on Wiley Online Library for rules of use; OA articles are governed by the applicable Creative Commons License

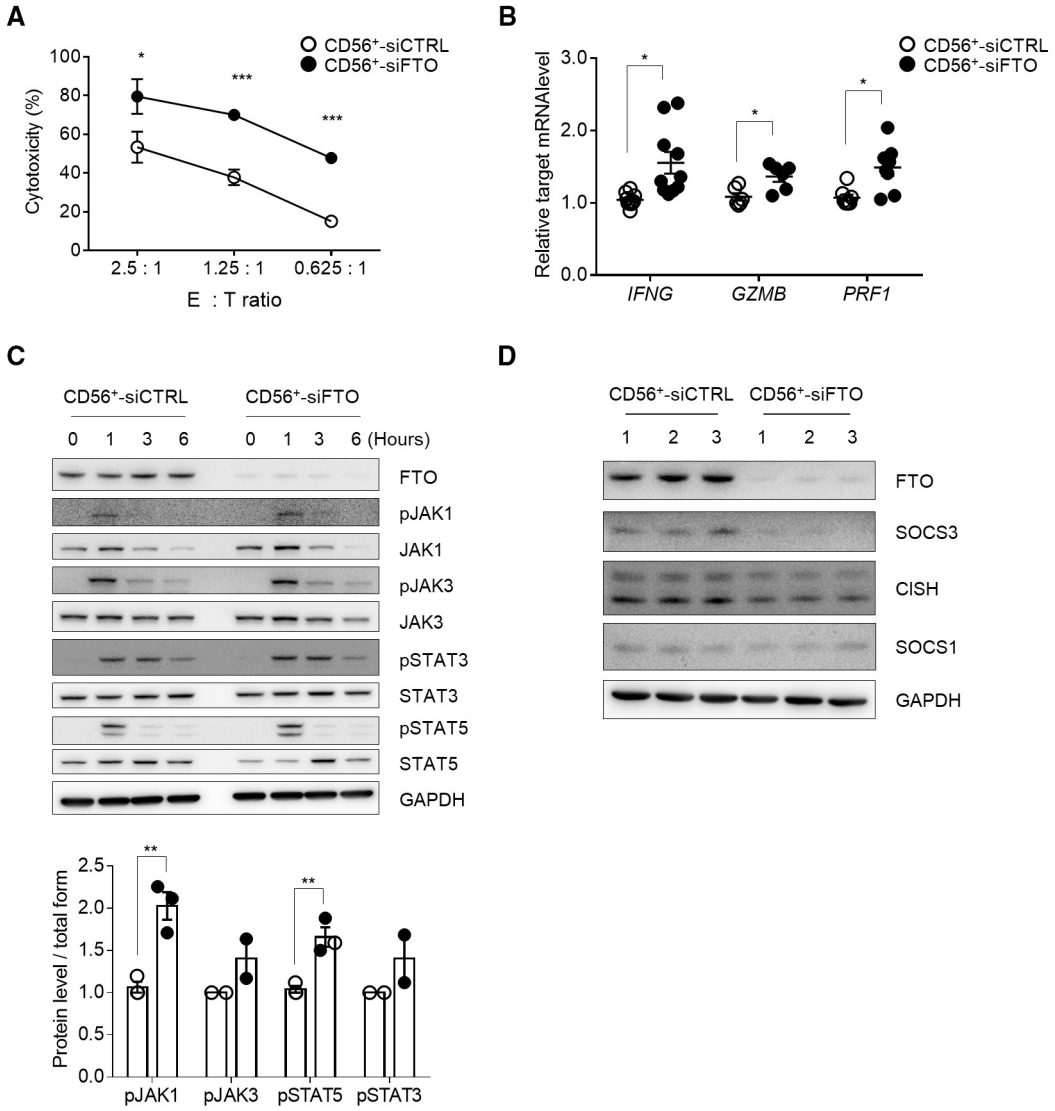

Figure 5. Activity of FTO-deficient CD3$^-$CD56$^+$ NK cells derived from umbilical cord blood is enhanced.

A K562 leukemia cell-killing activity by CD56$^+$-siCTRL or CD56$^+$-siFTO cells was measured by calcein AM-based cytotoxicity assays at the indicated NK:K562 (E:T) ratio.

B Relative mRNA expression levels of JAK/STAT target genes, *IFNγ* ($n = 10$ biological replicates), *GZMB* ($n = 6$ biological replicates), and *PRF1* ($n = 8$ biological replicates) were determined by qPCR in CD56$^+$-siCTRL or CD56$^+$-siFTO cells.

C Western blotting of CD56$^+$-siCTRL or CD56$^+$-siFTO cells incubated with 20 ng/ml IL-15 and 20 ng/ml IL-21 for the indicated times was performed. Cells were lysed and analyzed by immunoblotting with antibodies to the indicated phosphorylated (p-) and total proteins ($n = 2 \sim 3$). Data are representative of three times independent experiments with similar results. The protein levels were expressed as the relative band density of the corresponding protein (lower).

D Western blotting for the detection of CISH, SOCS1, and SOCS3 was performed in CD56$^+$-siCTRL or CD56$^+$-siFTO cells ($n = 3$/group).

Data information: Error bars for panel (A) are ± s.d. based on three technical replicates. Error bars for panels (B and C) are ± s.e.m. For panels (A), data are representative of three times independent experiments with similar results. For panels (C), The protein levels were expressed as the relative band density of the corresponding protein on the lower. Significance was determined using the Student's *t*-tests (A, C) or Mann–Whitney *U* test (B): ***$P < 0.001$; **$P < 0.01$; *$P < 0.05$. Source data are available online for this figure.

et al, 2017). Nevertheless, its relationship with immune cell activity has not been reported to date. In the present study, we characterized the role of FTO in NK cell biology. *Fto*$^{-/-}$ mice displayed prolonged survival against lymphoma and resistance to melanoma tumor metastasis. NK92-siFTO cells were hypersensitive to the IL-2-driven phosphorylation of JAK1 and JAK3, with corresponding increases in NK cytotoxicity, cytokine production, and survival. Furthermore, the expression of the activating receptor NKp30 was increased in the NK92-siFTO cells, leading to increased NK cell activity (Fig 7).

mRNA levels are tightly regulated by both transcription and degradation (Tani & Akimitsu, 2012). Rates of transcription mainly control mRNA abundance; however, a small number of mRNAs, especially immediate-early inducible genes, are closely regulated by

© 2023 The Authors

14693178, 0, Downloaded from https://www.embopress.org/doi/10.15252/embr.202255681 by Korea Research Institute Of, Wiley Online Library on [06/03/2023]. See the Terms and Conditions (https://onlinelibrary.wiley.com/terms-and-conditions) on Wiley Online Library for rules of use; OA articles are governed by the applicable Creative Commons License

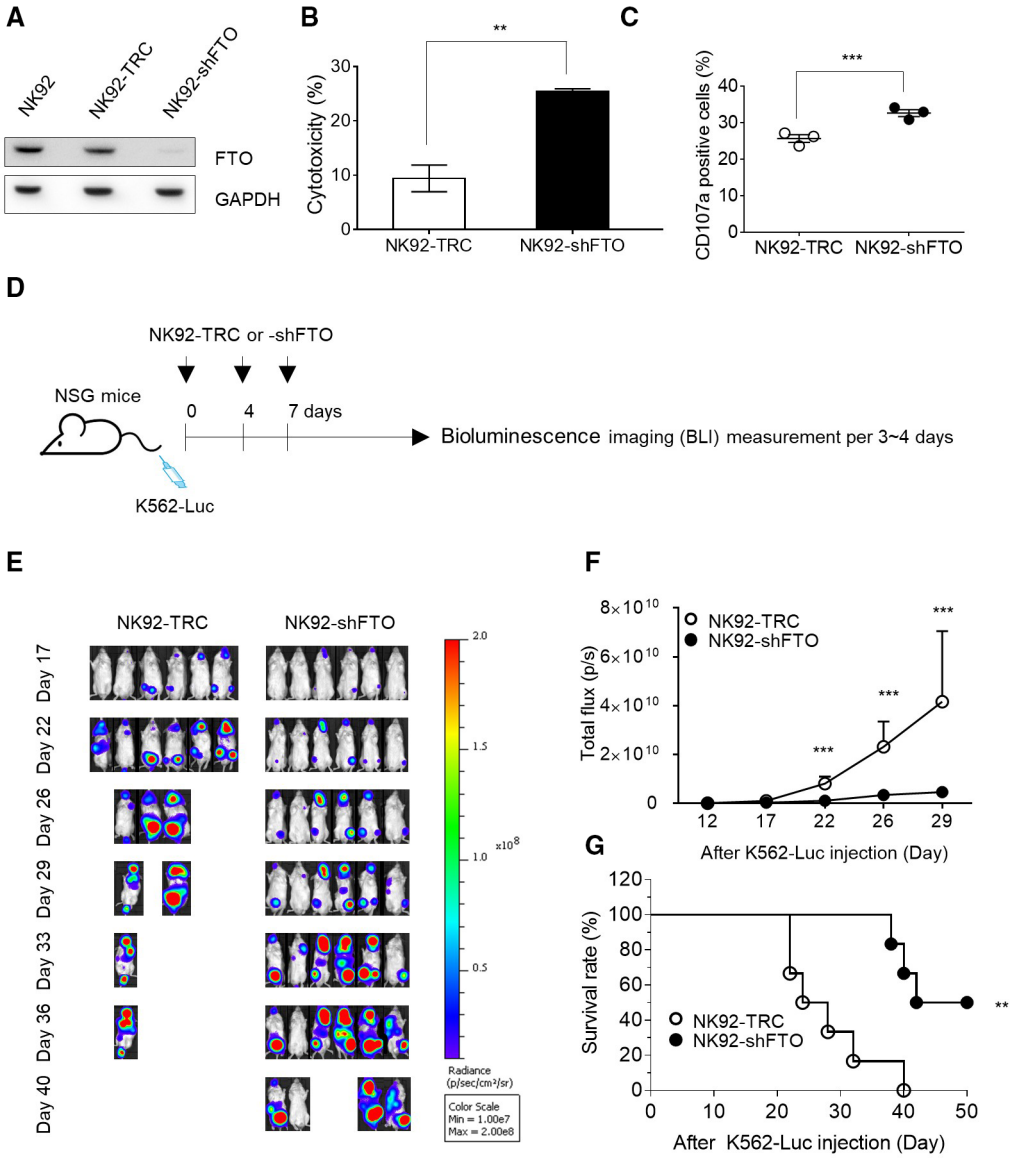

Figure 6. FTO-deficient NK cells enhance the antitumor responses against K562 leukemia.

A Western blotting for the detection of FTO was performed in NK92-TRC or NK92-shFTO cells.

B K562-Luc cell-killing activity by NK92-TRC or NK92-shFTO cells was measured by calcein AM-based cytotoxicity assay (E:T ratio = 1:0.625).

C Degranulation was measured by flow cytometry ($n = 3$ biological replicates, E:T ratio = 2:1).

D The mouse experimental scheme. K562-Luc cells were injected, and then, NK92-TRC or NK92-shFTO was transfused three times into NOD/Shi-*scid*/IL-2Rγ^{null} (NOG) mice ($n = 6$/group).

E The images of the ventral bioluminescence (BLI) following the injection of NK92-TRC or NK92-shFTO cells.

F The values of the ventral BLI were plotted.

G The survival curves after the injection of K562-Luc cells.

Data information: Error bars for panel (B) are ± s.d. based on three technical replicates. Error bars for panels (C and F) are ± s.e.m. For panels (A and B), data are representative of three times independent experiments with similar results. Significance was determined using the Student's *t*-tests (B, C, F) or the Mantel–Cox test (G): ***$P < 0.001$; **$P < 0.01$.

Source data are available online for this figure.

mRNA degradation (Rabani *et al*, 2014). Post-transcriptional modification is helpful for rapid degradation. Among various post-transcriptional modifications, m^{6}A is the most common and vital epitranscriptomic mark. Although m^{6}A RNA modification plays fundamental roles in almost every aspect of mRNA metabolism, it mainly affects RNA degradation (Shulman & Stern-Ginossar, 2020). SOCS family genes are well-known immediate-early genes induced by IL-2/15 or IL-17 stimulation (Li *et al*, 2017b). Therefore, the

© 2023 The Authors

14693178, 0, Downloaded from https://www.embopress.org/doi/10.15252/embr.202255681 by Korea Research Institute Of, Wiley Online Library on [06/03/2023]. See the Terms and Conditions (https://onlinelibrary.wiley.com/terms-and-conditions) on Wiley Online Library for rules of use; OA articles are governed by the applicable Creative Commons License

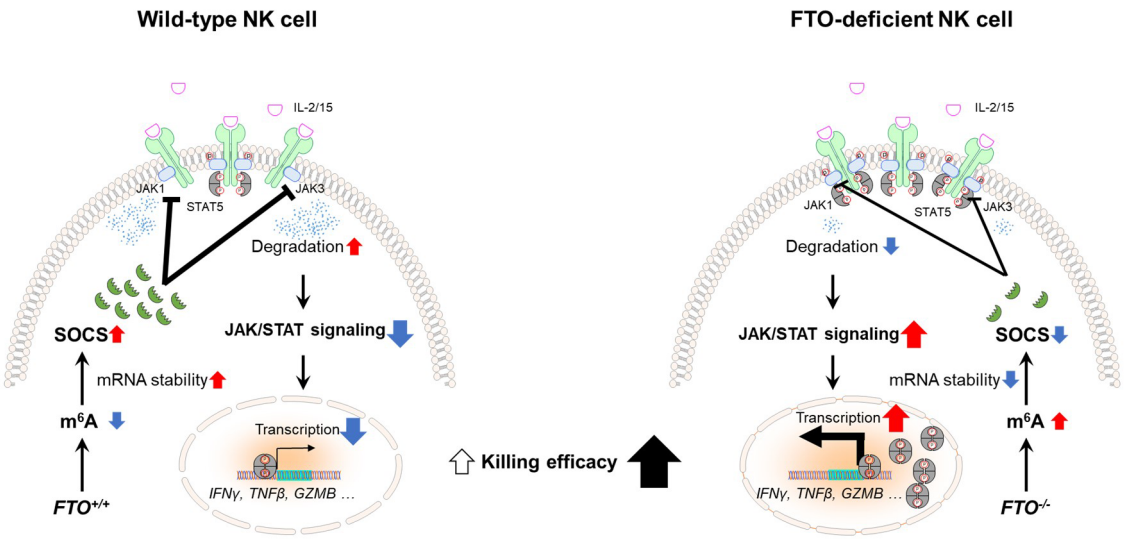

Figure 7. FTO is a crucial negative regulator of IL-2/15-induced JAK/STAT signaling.

Overview of the proposed model. In FTO-deficient NK cells, the expression levels of SOCS family genes are low due to high levels of m^{6}A RNA methylation in the mRNA. Low SOCS family gene expression promotes the JAK/STAT signaling, thereby increasing the efficacy of NK cell killing.

degradation of SOCS family genes may also be related to m^{6}A RNA methylation for immediate reactions to stimuli.

Previous reports have shown that m^{6}A in the mRNA of SOCS family genes regulates T cell homeostasis by regulating mRNA stability via the m^{6}A writers METTL3 and METTL14 (Li *et al*, 2017b; Tong *et al*, 2018). However, the effects of m^{6}A erasers on other immune cells are not well-known (Gu *et al*, 2020). We found that SOCS family proteins, especially *SOCS3*, are downregulated in mouse NK cells lacking the m^{6}A eraser FTO and in NK92-siFTO cells. By MeRIP–qPCR and a reporter assay, we found that mRNAs of SOCS family genes have m^{6}A modifications, which are removed by FTO, thus reducing mRNA stability. In addition, we observed that these regulatory effects also affect NK cell activity and provide a potential clinical approach. The opposite findings were obtained using the m^{6}A eraser, clearly demonstrating the importance of m^{6}A in immune cells. In addition, we verified that SOCS family genes are m^{6}A target genes and that m^{6}A dynamics are regulated not only by m^{6}A writers but also by m^{6}A erasers. Additionally, cytokine signaling is a key signaling pathway in a variety of immune cells (Van der Meide & Schellekens, 1996). As well as IL-2/15, IL-7 is a typical gamma chain cytokine, involving a similar signaling cascade (Ma *et al*, 2006). Just as IL-7 mainly regulates cellular homeostasis in T cells, in NK cells, IL-2/15 primarily regulates the activity of NK cells (Becknell & Caligiuri, 2005). In this way, even if intermediate signaling factors are shared, signaling outputs differ among cells. Therefore, even the already-known m6A-modified mRNA is considered to be sufficiently meaningful.

A recently published paper identified the role of m^{6}A in NK cells using the m^{6}A writer METTL3 (Song *et al*, 2021) and the m^{6}A reader YTHDF2 (Ma *et al*, 2021). According to the reported papers, METTL3 regulates responsiveness to IL-15, and YTHDF2 forms a positive feedback loop with STAT5 to regulate IL-15 signaling. Here, we emphasize that FTO negatively regulates IL-2/15-driven JAK/STAT signaling. All three results have different m^{6}A target genes and detailed mechanisms, but all describe that they regulate the sensitivity of IL-2/15 signaling to regulate NK cell homeostasis and antitumor immunity. These results suggest that m^{6}A RNA modification is essential in NK cell biology.

As reported, m^{6}A RNA methylation is present in about 25% of transcripts in the eukaryotic transcriptome (Dominissini *et al*, 2012). This means that m^{6}A demethylation by FTO is not limited to the SOCS family genes in NK cells. We focused only on cytokine-induced NK cell activation. When treated with IL-2/15, FTO-deficient NK cells showed increases in JAK/STAT signaling (Fig 3). However, differences in other cytokines, signaling molecules, and cellular signal transduction through direct contact with target cells were not considered. Therefore, for a broader understanding of the role of FTO in NK cells, additional studies covering a wider range of conditions and signaling factors are needed.

In summary, we showed that FTO is a crucial negative regulator of IL-2/15-driven JAK/STAT signaling in NK cells by removing m^{6}A in the mRNA of SOCS family genes, especially *SOCS3*. FTO-deficient NK cells displayed increased tumor-killing activity, cytokine production, and cell viability. Accordingly, *Fto*$^{-/-}$ mouse splenic NK cells were resistant to experimental melanoma tumor metastasis and FTO-deficient NK cells showed an enhanced antitumor response to K562 leukemia (Fig 7). Adoptive transfer of allogeneic NK cells is a potential immunotherapeutic strategy for a variety of cancers (Guillerey *et al*, 2016). Little is known about the usage of an immune checkpoint inhibitor for NK cells. Antibodies for TIGIT, KIR, TIM-3, LAG-3, and NKG2A are undergoing clinical trials (Cao *et al*, 2020). It has also been reported that CISH could be a potent checkpoint in NK cells (Delconte *et al*, 2016). Therefore, we thought that FTO could be used as an immune checkpoint for NK cells and could provide the basis for a new immunotherapeutic strategy for allogeneic NK cell therapies.

© 2023 The Authors

14693178, 0, Downloaded from https://www.embopress.org/doi/10.15252/embr.202255681 by Korea Research Institute Of, Wiley Online Library on [06/03/2023]. See the Terms and Conditions (https://onlinelibrary.wiley.com/terms-and-conditions) on Wiley Online Library for rules of use; OA articles are governed by the applicable Creative Commons License

Materials and Methods

Mice

Fto knockout mice were generated by GH bio (Republic of Korea). The mouse *Fto* gene (gene ID: 26383) consists of nine exons. $Fto^{-/-}$ mice were generated by using CRISPR/Cas9 system (pT7 plasmid). It was designed to induce deleted mutation in the first exon with the start codon (Fig EV1A–C). The single-guide RNA (sgRNA) was selected from CHOPCHOP program (http://chopchop.cbu.uib.no, target 1: GGCGAGGGGGAACACGGCCCACGG, target 2: GACCGCGGAGGAACGAGAGCGG). The specific primer sequences for genotyping are as follows. 5′-CTGCTAGCTGACTGGAGAAAT-3′, 5′-ATATGAATTCACAGCACAGACG-3′. $Fto^{-/-}$ mice were maintained on a C57BL/6 background. $Fto^{+/+}$ refers to C57BL/6 wild-type control mice, which were purchased from DOO YEOL Biotech (Republic of Korea). For bioluminescence assay, male NOG mice (NOD.Cg-Prkdcscid Il2rgtm1Sug/Jic, 5–8 weeks) were purchased from saeronbio (Republic of Korea). All mice were bred and maintained under Specific Pathogen Free conditions. Animal experiments complied with the guidelines (approval ID: KRIBB-AEC-20032, -20327, -21009) of the Institutional Animal Care and Use Committee (IACUC) of the Korea Research Institute of Bioscience and Biotechnology (KRIBB). Experiments were performed in accordance with institutional guidelines for animal care (National Institutes of Health, Bethesda, MD, USA). Male and female mice were used between the ages of 8–12 weeks.

Tumor metastasis and NK depletion

Groups of 9–10 mice per experiment were used for tumor metastasis assay with NK cell depletion. Single-cell suspension of 1×10^5 B16F10 melanoma cells in 200 μl of PBS was injected intravenously into the tail vein of $Fto^{+/+}$ or $Fto^{-/-}$ mice on day 0. In the NK cell depletion assay, $Fto^{+/+}$ mice or $Fto^{-/-}$ mice were intraperitoneally injected with either 100 μg anti-mouse IgG2a isotype control (BioXCell, #BE0085) or 100 μg anti-mouse NK1.1 antibody (BioXCell, #BE0036) per mouse on days −4, −1 and 2. The efficiency of NK cell depletion was measured by flow cytometry.

B16F10 xenograft mouse model

2×10^5 B16F10 melanoma cells in 200 μl of PBS were injected subcutaneously into the flank of $Fto^{+/+}$ or $Fto^{-/-}$ mice. The tumor size was measured every 3–4 days with calipers and was calculated using the formula [length × width^2 × 0.5]. Seventeen days after B16F10 inoculation, the tumor was extracted.

Purification and culture of mouse splenic NK cells

Mouse natural killer cells were harvested from the spleen and single-cell suspensions prepared by forcing of the spleen through 70 μm Cell Strainer (FALCON). NK cells were purified using mouse NK Cell Isolation Kit II (Miltenyi Biotec) according to the manufacturer's instructions. NK cells were expanded for 1–2 days by culture in RPMI-1640 supplemented with 10% fetal bovine serum (FBS), 1% streptomycin and penicillin, recombinant hIL-2 (40 ng/ml, Peprotech) and hIL-15 (40 ng/ml; Peprotech).

Cell culture

The NK-92 (human natural killer cell line, ATCC®CRL-2407™), K562 (human leukemia cell line, ATCC®CCL-243™), B16F10 (mouse skin melanoma cell line, ATCC®CRL-6475™), YAC1 (mouse lymphoma cell line, ATCC®TIB-160™) and EL4 (mouse lymphoma cell line, ATCC®TIB-39™) were purchased from American Type Culture Collection (Manassas, VA, USA). The K562-Luc cell lines were generated by transduction with a lentiviral vector (pCDH-CMV-MCS-T2A GFP EF1-Puro) encoding luciferase and GFP. The NK-92 cells were grown in an alpha minimum essential medium, which contained 12.5% fetal bovine serum (FBS), and 12.5% horse serum. To prepare the complete growth medium, the following components were added to the medium prior to use: 0.2 mM inositol, 0.1 mM 2-mercaptoethanol, 0.02 mM folic acid, and 200 U/ml recombinant IL-2 (Peprotech, Cat. 200–02). K562, K562-Luc, and YAC1 cell lines were grown in RPMI-1640 medium, which contained 10% FBS, and 1% streptomycin and penicillin. B16F10 and EL4 cell lines were grown in DMEM medium (high glucose), which contained 10% FBS, and 1% streptomycin and penicillin. In case of human, primary NK cells derived from umbilical cord blood (UCB). Samples of human cord blood were obtained from umbilical veins of normal and full-term infants after written informed consent by their mothers, and the protocol was approved by the guidance of the electronic Institutional Review Board (P01-201906-41-001). Primary human $CD3^-$ NK cells were isolated from UCB mononuclear cells using RosetteSep (Stem Cell Technologies), which depletes the cluster of differentiation $CD3^+$ T cells (≤ 5% $CD3^+$ cells) and red blood cells. The cells were cultured in α-Minimal Essential Medium (Welgene) with IL-15 (100 U/ml), IL-21 (100 U/ml), and 1 μM of hydrocortisone until the $CD56^+$ mononuclear cells became more than 80% (~12 days). Mycoplasma contamination was tested with the commercially available mycoplasma detection kit (iNtRON, #25239).

Real-time quantitative PCR (RT–qPCR) and m^{6}A methylated RNA immunoprecipitation (MeRIP)–qPCR

Total ribonucleic acid (RNA) was extracted with the use of Trizol (Thermo Fisher, #15596026) according to the manufacturer's instructions. Total RNA was reverse-transcribed using a complementary deoxyribonucleic acid (cDNA) synthesis kit (Toyobo, #FSK-101) and RT-qPCR was conducted with the use of a Dice TP800 thermal real-time PCR system with SFC green qPCR master mix (SFC, #pgm1005). Extracted cellular RNA was also used for MeRIP assay. MeRIP (#17-10499) kits were purchased from Merck and performed according to the manufacturer's instructions. All the measurements were normalized to the housekeeping gene GlycerAldehyde-3-Phosphate Dehydrogenase (*GAPDH*) and input control. Each condition had three biological replicates and measurements were performed in duplicate. The gene-specific primer sequences are listed below.

Human *GAPDH* – F: 5′-GAGTCAACGGATTTGGTCGT-3′ and R: 5′-TTGATTTTGGAGGGATCTCG-3′; human *METTL3* – F: 5′-CTTG CATGGATTCTGAGGCC-3′ and R: 5′-GTCAGCCATCACAACTGCAA-3′; human FTO – F: 5′-CGGTATCTCGCATCCTCATT-3′ and R: 5′-GG CAGCAAGTTCTTCCAAAG-3′; human *IFNγ* – F: 5′-TCCCATGGGTTG

© 2023 The Authors

14693178, 0, Downloaded from https://www.embopress.org/doi/10.15252/embr.202255681 by Korea Research Institute Of, Wiley Online Library on [06/03/2023]. See the Terms and Conditions (https://onlinelibrary.wiley.com/terms-and-conditions) on Wiley Online Library for rules of use; OA articles are governed by the applicable Creative Commons License

TGTGTTTA-3′ and R: 5′-AAGCACCAGGCATGAAATCT-3′; human *TNFα* – F: 5′-AGGACCAGCTAAGAGGGAGA-3′ and R: 5′-CCCGGATC ATGCTTTCAGTG-3′; human *GZMB* – F: 5′-CCCTGGGAAAACACT CACACA-3′ and R: 5′-CACAACTCAATGGTACTGTCGT-3′; human *CISH* – F: 5′-CCTGGCCACCTGAACTGTAT-3′ and R: 5′-CCCTCAAC AAGGGGTCACTA-3′; human *SOCS1* – F: 5′- CTGGGATGCCGTGTT ATTTT-3′ and R: 5′-TAGGAGGTGCGAGTTCAGGT-3′; human *SOC S2* – F: 5′-GTGCAAGGATAAGCGGACAG-3′ and R: 5′-GGTAAA GGCAGTCCCCAGAT-3′; human *SOCS3* – F: 5′-ATCCTGGTGACAT GCTCCTC-3′ and R: 5′-CAAATGTTGCTTCCCCCTTA-3′; human *BCl-2* – F: 5′-CTGCACCTGACGCCCTTCACC-3′ and R: 5′-CACATGA CCCCACCGAACTCAAAGA-3′; human *PIM1* – F: 5′-CCGAGTGTATA GCCCTCCAG-3′ and R: 5′-GGGCCAAGCACCATCTAATG-3′; human *BCL-XL* – F: 5′-TCCCAGCTTCACATAACCCC-3′ and R: 5′-TGCATCTCCTTGTCTACGCT-3′; human *MYC* – F: 5′-AACACACA ACGTCTTGGAGC-3′ and R: 5′-GCACAAGAGTTCCGTAGCTG-3′; mouse *Gapdh* – F: 5′-ATGGTGAAGGTCGGTGTGAA-3′ and R: 5′-TGGAAGATGGTGATGGGCTT-3′; mouse *Cish* – F: 5′-CTCTGGG ACATGGTCCTTTG-3′ and R: 5′-GGCATCTTCTGTAGGTGCTG-3′; mouse *Socs1* – F: 5′-GTCCTGCCGCCAGATGAG-3′ and R: 5′-GCCAA CAGACCCCAAGGAG-3′; mouse *Socs2* – F: 5′-CTGCGCGAGCT CAGTCAAAC-3′ and R: 5′-GTCTGAATGCGAACTATCTC-3′; mouse *Socs3* – F: 5′-AGATTTCGCTTCGGGACTAG-3′ and R: 5′-GGAGCC AGCGTGGATCTGC-3′; mouse *Ifng* – F: 5′-TTCTTCAGCAACAGC AAGGC-3′ and R: 5′-ACTCCTTTTCCGCTTCCTGA-3′; mouse *Gzmb* – F: 5′-AGAACAGGAGAAGACCCAGC-3′ and R: 5′-GCTTCACATTG ACATTGCGC-3′.

m^{6}A dot blot and m^{6}A ELISA assay

Total RNA was extracted as described above. Extracted cellular RNA was used for m^{6}A dot blot and m^{6}A ELISA assay. In the m^{6}A dot blot assay, dropped 2 μl of total RNA was onto the positively charged nylon membrane (Merck) and fixed by boiling at 80°C for 2 h. Then, washed membrane in PBST (1× PBS, 0.05% Tween-20) for 10 min. Incubated the membrane with anti-m^{6}A antibody (Synaptic Systems, 202003) in 10% skim milk and then washed the membrane. After wash, incubated with peroxidase (HRP)-conjugated goat anti-rabbit (Thermo Fisher, #31460) for 1 h, and then, the signal band detected using SuperSignal West Pico Chemiluminescent Substrate (Thermo Fisher, #34078). m^{6}A ELISA assay (#P-9005-96) kits were purchased from Epigentek and performed according to the manufacturer's instructions in triplicate.

Flow cytometry

Single-cell suspensions were stained with the appropriate antibodies for 20 min on ice in a binding buffer (PBS with 2% FBS and 1 mM EDTA) and analyzed by a fluorescence-activated cell sorter (FACS) Canto II and FlowJo software (BD Biosciences). For apoptotic assays, cells were stained with the fluorescein isothiocyanate (FITC) Annexin V and propidium iodide (PI) according to the BD Apoptosis Detection Kit II manual. Antibodies specific for CD3 (#5607771), CD4 (#553046), CD8 (#553035), NK1.1 (#551114), CD107a (#555801), CD56 (#562751), NKG2D (558071), NKp30 (#558407), NKp44 (#558563), NKp46 (558051) and CD25 (#555434) were purchased from BD Pharmingen and used at 1:100.

Calcein AM-based cytotoxicity

NK cell cytotoxicity was measured with the Calcein release assay. Target cancer cells were labeled with Calcein AM (Thermo Fisher, #C1430) for 1 h at 37°C. The labeled target cells (1×10^4 cells) and serially diluted effector NK cells were then co-cultured in 96-well round-bottom plates for 4 h at 37°C. Released Calcein into the supernatant was measured using a multimode microplate reader (Molecular Devices, San Jose, CA, USA). Maximum release was simulated based on the addition of 1% Triton X-100 to the labeled target cells, and spontaneous release was simulated by adding culture media to the labeled target cells. The percentage of specific lysis was calculated according to the following formula:

$$(\text{sample release} - \text{spontaneous release}) / (\text{maximum release} - \text{spontaneous release}) \times 100.$$

Cytokine ELISA analysis

Cultured supernatants were used for cytokine ELISA analyses. Human IFNγ (#88-7316-88), human TNFα ELISA (#88-7346-88), mouse IFNγ (#88-7314-86), and mouse TNFα ELISA (#88-7324-22) kits were purchased from Invitrogen and performed according to the manufacturer's instructions in triplicate.

Western blotting

Cells were lysed in protein lysis buffer (Roche, #4719956001) with protease and phosphatase inhibitor (Roche, #4906837001). Lysates were clarified by centrifugation at 15,814 *g* for 10 min at 4°C. Protein concentrations were measured by the BCA protein assay kit (Thermo Fisher, #23225). The lysates were loaded on 10% SDS–PAGE gels and transferred to 0.45 μm PVDF membrane (Merck Millipore, #IPVH00010). After transfer, the membrane was incubated with primary antibodies specific to the following: GAPDH (#5174), pJAK1 (Y1022/1023, #3331), JAK1 (#3344), pJAK3 (Y980/981, #5031), JAK3 (#8863), pSTAT5 (Y694, #9359), STAT5 (Santa Cruz Biotechnology, #sc-74442), pSTAT3 (Y705, #5031), STAT3 (#9139), FTO (#45980), METTL3 (Proteintech, #15073-1-AP), GZMB (#3707), CISH (#8731), SOCS1 (#3950), SOCS3 (#2923), pAKT (T308, #9275), AKT (#9272), pERK (T202/Y204, #9101), ERK (#9102), and serotonin N-acetyltransferase (AANAT, Abcam, #ab3506). Primary antibodies were purchased from Cell Signaling Technology (CST) unless stated otherwise. After incubation with peroxidase (HRP)-conjugated goat anti-rabbit (Thermo Fisher, #31460) or anti-mouse IgG (Thermo Fisher, #31430), the signal band was detected using SuperSignal West Pico Chemiluminescent Substrate (Thermo Fisher, #34078).

Transfection and reporter assay

In small interfering RNA (siRNA) transfection, 1×10^6 NK cells were transfected with one of either the siRNA control or siFTO (GGUUAGGAUCCAAGGCAAA+dTdT) at concentrations of 10 μM in 100 μl opti-MEM media (Thermo Fisher, #31985070) per one cuvette using NEPA21 electroporator (NepaGene) according to the manufacturer's instruction. pcNAT reporter plasmid has been previously described. To construct reporter plasmids pcNAT-human *SOCS3*

© 2023 The Authors

14693178, 0, Downloaded from https://www.embopress.org/doi/10.15252/embr.202255681 by Korea Research Institute Of, Wiley Online Library on [06/03/2023]. See the Terms and Conditions (https://onlinelibrary.wiley.com/terms-and-conditions) on Wiley Online Library for rules of use; OA articles are governed by the applicable Creative Commons License

3'UTR and –human *CISH* 3'UTR, 3'UTR of the human *SOCS3* and *CISH* were amplified by PrimeSTAR MAX DNA polymerase (Takara, #R045A) using a specific primer (*SOCS3* 3'TUR – F: AAGAATTCGGGGTAAAGGGCGCAAAG, R: AACTCGAGGTTTTT-CATTAAAAAATAGTGCTCTTTATTAT, *CISH* 3'UTR – F: AAGAATT CCTGTACGGGGCAATCTGC, R: AACTCGAGACACAACTGAAAAT CGGCC). The PCR products were cloned into the EcoRI and XhoI site of the pcNAT plasmid. Plasmid sequences were confirmed by sequencing (Macrogen). For reporter assay, HEK-293T cells were co-transfected with 3 μg of reporter plasmid with either 100 nM siRNA control (Bioneer) or siFTO using TransIT-X2 transfection reagent (Mirus, #MIR6005) according to the manufacturer's manual. Transfected cells were further grown for 24 h before harvesting.

shRNA construct and lentivirus infection

To construct shRNA plasmid, used pLKO.1 TRC plasmid (Addgene, #10878) according to the manufacturer's instruction. The sequence of shFTO was taken from the sequence of siFTO. To generate the lentivirus, transfect expression vector, pLKO.1-shFTO and packaging vector, psPAX2 and enveloping vector, pMD2.G to HEK-293T cells using TransIT-2020 transfection reagents (Mirus, #.MIR5405). After 3 days, collect the supernatants and condensate the virus by ultra-centrifugation 77,175 *g* for 2 h. Extracted viruses are infected to the NK92 with 8 μg/ml protamine sulfate and infected NK92 cells are selected by using puromycin (3 μg/ml).

Mouse bioluminescence imaging

To generate K562 cells expressing luciferase (pCDH-CMV-MCS-T2A GFP EF1-PURO), extracted viruses are infected to the K562 cell according to the above method. The *in vivo* mouse bioluminescence measurement using the IVIS Imaging System (Caliper Life Sciences). Before detection of the luciferase activity in mouse, mice were anesthetized with 1 ~ 3% isoflurane, and intraperitoneal inject to mouse at 150 mg D-luciferin (PerkinElmer, #122799) per kg of mouse body weight. After 10–15 min, luciferase activity expressed by K562-Luc was detected by auto-exposure with a maximum exposure time of 1 min. And it was analyzed by using Living Image software (PerkinElmer). Average radiance (photons/s/cm^2/steradian) was calculated using standardized regions of interest across imaging sessions. Total flux was calculated in photons/s.

Statistical analyses

To exclude subjective bias, randomization procedures and blind testing were performed. *In vitro* experimental samples were tested in duplicate or triplicate, and experiments were performed two or three times independently. Mouse experiments were repeated two independently with similar results. Statistical significance was assessed with the Student's *t*-tests or the Mann–Whitney *U* or Mantel–Cox using GraphPad Prism (Version 7.0, GraphPad Software). The data normality test was performed using the "Kolmogorov–Smirnov test." If the data were normally distributed, statistical tests were performed using the "Student's *t*-test" of the two-sided two-sample *t*-test. Statistical tests were performed using the "Mann–Whitney *U* test" if the data were not normally distributed. For mouse survival rate, the "Log-rank (Mantel–Cox) test" was used. Values of $P < 0.05$ were considered to be statistically significant.

Data availability

All data are available in the main manuscript or the supplementary materials. All data and materials used in this manuscript are available from the authors upon reasonable request. No primary datasets have been generated and deposited.

Expanded View for this article is available online.

Acknowledgements
We thank Dr. Hyunjoon Kim for technical support and manuscript comments and troubleshooting advice. This work was supported by KRIBB Research Initiative Program, the National Research Council of Science and Technology (NST) grant (CAP-18-02-KRIBB), the National Research Foundation grant (2022M3E5F1016693), and Korea Drug Development Fund (HN21C0117) by the Korea government.

Author contributions
Seok-Min Kim: Conceptualization; formal analysis; investigation; visualization; methodology; writing – original draft; writing – review and editing. **Se-Chan Oh:** Investigation. **Sun-Young Lee:** Investigation. **Ling-Zu Kong:** Investigation. **Jong-Hee Lee:** Investigation. **Tae-Don Kim:** Conceptualization; supervision; project administration; writing – review and editing.

Disclosure and competing interests statement
The authors declare that they have no conflict of interest.

References

Baker BJ, Akhtar LN, Benveniste EN (2009) SOCS1 and SOCS3 in the control of CNS immunity. *Trends Immunol* 30: 392–400

Bald T, Krummel MF, Smyth MJ, Barry KC (2020) The NK cell-cancer cycle: advances and new challenges in NK cell-based immunotherapies. *Nat Immunol* 21: 835–847

Becknell B, Caligiuri MA (2005) Interleukin-2, interleukin-15, and their roles in human natural killer cells. *Adv Immunol* 86: 209–239

Cao Y, Wang X, Jin T, Tian Y, Dai C, Widarma C, Song R, Xu F (2020) Immune checkpoint molecules in natural killer cells as potential targets for cancer immunotherapy. *Signal Transduct Target Ther* 5: 250

Chen M, Wei L, Law CT, Tsang FH, Shen J, Cheng CL, Tsang LH, Ho DW, Chiu DK, Lee JM *et al* (2018) RNA N6-methyladenosine methyltransferase-like 3 promotes liver cancer progression through YTHDF2-dependent posttranscriptional silencing of SOCS2. *Hepatology* 67: 2254–2270

Cheng Y, Luo H, Izzo F, Pickering BF, Nguyen D, Myers R, Schurer A, Gourkanti S, Bruning JC, Vu LP *et al* (2019) M(6)a RNA methylation maintains hematopoietic stem cell identity and symmetric commitment. *Cell Rep* 28: 1703–1716

Darnell RB, Ke S, Darnell JE Jr (2018) Pre-mRNA processing includes N(6) methylation of adenosine residues that are retained in mRNA exons and the fallacy of "RNA epigenetics". *RNA* 24: 262–267

Delconte RB, Kolesnik TB, Dagley LF, Rautela J, Shi W, Putz EM, Stannard K, Zhang JG, Teh C, Firth M *et al* (2016) CIS is a potent checkpoint in NK cell-mediated tumor immunity. *Nat Immunol* 17: 816–824

© 2023 The Authors

14693178, 0, Downloaded from https://www.embopress.org/doi/10.15252/embr.202255681 by Korea Research Institute Of, Wiley Online Library on [06/03/2023]. See the Terms and Conditions (https://onlinelibrary.wiley.com/terms-and-conditions) on Wiley Online Library for rules of use; OA articles are governed by the applicable Creative Commons License

Desrosiers R, Friderici K, Rottman F (1974) Identification of methylated nucleosides in messenger RNA from Novikoff hepatoma cells. *Proc Natl Acad Sci USA* 71: 3971–3975

Dina C, Meyre D, Gallina S, Durand E, Korner A, Jacobson P, Carlsson LM, Kiess W, Vatin V, Lecoeur C *et al* (2007) Variation in FTO contributes to childhood obesity and severe adult obesity. *Nat Genet* 39: 724–726

Ding C, Xu H, Yu Z, Roulis M, Qu R, Zhou J, Oh J, Crawford J, Gao Y, Jackson R *et al* (2022) RNA m(6)a demethylase ALKBH5 regulates the development of gammadelta T cells. *Proc Natl Acad Sci USA* 119: e2203318119

Dominissini D, Moshitch-Moshkovitz S, Schwartz S, Salmon-Divon M, Ungar L, Osenberg S, Cesarkas K, Jacob-Hirsch J, Amariglio N, Kupiec M *et al* (2012) Topology of the human and mouse m6A RNA methylomes revealed by m6A-seq. *Nature* 485: 201–206

Fan HQ, He W, Xu KF, Wang ZX, Xu XY, Chen H (2015) FTO inhibits insulin secretion and promotes NF-kappaB activation through positively regulating ROS production in pancreatic beta cells. *PLoS ONE* 10: e0127705

Fischer J, Koch L, Emmerling C, Vierkotten J, Peters T, Bruning JC, Ruther U (2009) Inactivation of the Fto gene protects from obesity. *Nature* 458: 894–898

Furlan M, Galeota E, de Pretis S, Caselle M, Pelizzola M (2019) m6A-dependent RNA dynamics in T cell differentiation. *Genes (Basel)* 10: 28

Fustin JM, Doi M, Yamaguchi Y, Hida H, Nishimura S, Yoshida M, Isagawa T, Morioka MS, Kakeya H, Manabe I *et al* (2013) RNA-methylation-dependent RNA processing controls the speed of the circadian clock. *Cell* 155: 793–806

Gotthardt D, Trifinopoulos J, Sexl V, Putz EM (2019) JAK/STAT cytokine signaling at the crossroad of NK cell development and maturation. *Front Immunol* 10: 2590

Gu X, Zhang Y, Li D, Cai H, Cai L, Xu Q (2020) N6-methyladenosine demethylase FTO promotes M1 and M2 macrophage activation. *Cell Signal* 69: 109553

Guillerey C, Huntington ND, Smyth MJ (2016) Targeting natural killer cells in cancer immunotherapy. *Nat Immunol* 17: 1025–1036

Han D, Liu J, Chen C, Dong L, Liu Y, Chang R, Huang X, Liu Y, Wang J, Dougherty U *et al* (2019) Anti-tumour immunity controlled through mRNA m(6)a methylation and YTHDF1 in dendritic cells. *Nature* 566: 270–274

Hilton DJ, Richardson RT, Alexander WS, Viney EM, Willson TA, Sprigg NS, Starr R, Nicholson SE, Metcalf D, Nicola NA (1998) Twenty proteins containing a C-terminal SOCS box form five structural classes. *Proc Natl Acad Sci USA* 95: 114–119

Hinney A, Nguyen TT, Scherag A, Friedel S, Bronner G, Muller TD, Grallert H, Illig T, Wichmann HE, Rief W *et al* (2007) Genome wide association (GWA) study for early onset extreme obesity supports the role of fat mass and obesity associated gene (FTO) variants. *PLoS ONE* 2: e1361

Huang Y, Su R, Sheng Y, Dong L, Dong Z, Xu H, Ni T, Zhang ZS, Zhang T, Li C *et al* (2019) Small-molecule targeting of oncogenic FTO demethylase in acute myeloid leukemia. *Cancer Cell* 35: 677–691

Huang H, Zhang G, Ruan GX, Li Y, Chen W, Zou J, Zhang R, Wang J, Ji SJ, Xu S *et al* (2022) Mettl14-mediated m6A modification is essential for germinal center B cell response. *J Immunol* 208: 1924–1936

Ivanova I, Much C, Di Giacomo M, Azzi C, Morgan M, Moreira PN, Monahan J, Carrieri C, Enright AJ, O'Carroll D (2017) The RNA m(6)a reader YTHDF2 is essential for the post-transcriptional regulation of the maternal transcriptome and oocyte competence. *Mol Cell* 67: 1059–1067

Jia G, Fu Y, Zhao X, Dai Q, Zheng G, Yang Y, Yi C, Lindahl T, Pan T, Yang YG *et al* (2011) N6-methyladenosine in nuclear RNA is a major substrate of the obesity-associated FTO. *Nat Chem Biol* 7: 885–887

Kan L, Grozhik AV, Vedanayagam J, Patil DP, Pang N, Lim KS, Huang YC, Joseph B, Lin CJ, Despic V *et al* (2017) The m(6)A pathway facilitates sex determination in drosophila. *Nat Commun* 8: 15737

Krebs DL, Hilton DJ (2001) SOCS proteins: negative regulators of cytokine signaling. *Stem Cells* 19: 378–387

Kwok CT, Marshall AD, Rasko JE, Wong JJ (2017) Genetic alterations of m(6)a regulators predict poorer survival in acute myeloid leukemia. *J Hematol Oncol* 10: 39

Lee H, Bao S, Qian Y, Geula S, Leslie J, Zhang C, Hanna JH, Ding L (2019) Stage-specific requirement for Mettl3-dependent m(6)A mRNA methylation during haematopoietic stem cell differentiation. *Nat Cell Biol* 21: 700–709

Li MO, Rudensky AY (2016) T cell receptor signalling in the control of regulatory T cell differentiation and function. *Nat Rev Immunol* 16: 220–233

Li A, Chen YS, Ping XL, Yang X, Xiao W, Yang Y, Sun HY, Zhu Q, Baidya P, Wang X *et al* (2017a) Cytoplasmic m(6)a reader YTHDF3 promotes mRNA translation. *Cell Res* 27: 444–447

Li HB, Tong J, Zhu S, Batista PJ, Duffy EE, Zhao J, Bailis W, Cao G, Kroehling L, Chen Y *et al* (2017b) M(6)a mRNA methylation controls T cell homeostasis by targeting the IL-7/STAT5/SOCS pathways. *Nature* 548: 338–342

Li Z, Qian P, Shao W, Shi H, He XC, Gogol M, Yu Z, Wang Y, Qi M, Zhu Y *et al* (2018) Suppression of m(6)a reader Ythdf2 promotes hematopoietic stem cell expansion. *Cell Res* 28: 904–917

Liu N, Dai Q, Zheng G, He C, Parisien M, Pan T (2015) N(6)-methyladenosine-dependent RNA structural switches regulate RNA-protein interactions. *Nature* 518: 560–564

Liu J, Zhang X, Chen K, Cheng Y, Liu S, Xia M, Chen Y, Zhu H, Li Z, Cao X (2019a) CCR7 chemokine receptor-inducible lnc-Dpf3 restrains dendritic cell migration by inhibiting HIF-1alpha-mediated glycolysis. *Immunity* 50: e615

Liu Y, Liu Z, Tang H, Shen Y, Gong Z, Xie N, Zhang X, Wang W, Kong W, Zhou Y *et al* (2019b) The N(6)-methyladenosine (m(6)a)-forming enzyme METTL3 facilitates M1 macrophage polarization through the methylation of STAT1 mRNA. *Am J Physiol Cell Physiol* 317: C762–C775

Lupo KB, Matosevic S (2019) Natural killer cells as allogeneic effectors in adoptive cancer immunotherapy. *Cancers (Basel)* 11: 769

Lv J, Zhang Y, Gao S, Zhang C, Chen Y, Li W, Yang YG, Zhou Q, Liu F (2018) Endothelial-specific m(6)a modulates mouse hematopoietic stem and progenitor cell development via notch signaling. *Cell Res* 28: 249–252

Ma A, Koka R, Burkett P (2006) Diverse functions of IL-2, IL-15, and IL-7 in lymphoid homeostasis. *Annu Rev Immunol* 24: 657–679

Ma S, Yan J, Barr T, Zhang J, Chen Z, Wang LS, Sun JC, Chen J, Caligiuri MA, Yu J (2021) The RNA m6A reader YTHDF2 controls NK cell antitumor and antiviral immunity. *J Exp Med* 218: e20210279

Mathiyalagan P, Adamiak M, Mayourian J, Sassi Y, Liang Y, Agarwal N, Jha D, Zhang S, Kohlbrenner E, Chepurko E *et al* (2019) FTO-dependent N(6)-Methyladenosine regulates cardiac function during remodeling and repair. *Circulation* 139: 518–532

Naeimi Kararoudi M, Elmas E, Lamb M, Chakravarti N, Trikha P, Lee DA (2018) Disruption of SOCS3 promotes the anti-cancer efficacy of primary NK cells. *Blood* 132: 5687

Niu Y, Zhao X, Wu YS, Li MM, Wang XJ, Yang YG (2013) N6-methyl-adenosine (m6A) in RNA: an old modification with a novel epigenetic function. *Genomics Proteomics Bioinformatics* 11: 8–17

Niu Y, Lin Z, Wan A, Chen H, Liang H, Sun L, Wang Y, Li X, Xiong XF, Wei B *et al* (2019) RNA N6-methyladenosine demethylase FTO promotes breast tumor progression through inhibiting BNIP3. *Mol Cancer* 18: 46

 © 2023 The Authors

14693178, 0, Downloaded from https://www.embopress.org/doi/10.15252/embr.202255681 by Korea Research Institute Of, Wiley Online Library on [06/03/2023]. See the Terms and Conditions (https://onlinelibrary.wiley.com/terms-and-conditions) on Wiley Online Library for rules of use; OA articles are governed by the applicable Creative Commons License

Panneerdoss S, Eedunuri VK, Yadav P, Timilsina S, Rajamanickam S, Viswanadhapalli S, Abdelfattah N, Onyeagucha BC, Cui X, Lai Z *et al* (2018) Cross-talk among writers, readers, and erasers of m(6)a regulates cancer growth and progression. *Sci Adv* 4: eaar8263

Rabani M, Raychowdhury R, Jovanovic M, Rooney M, Stumpo DJ, Pauli A, Hacohen N, Schier AF, Blackshear PJ, Friedman N *et al* (2014) High-resolution sequencing and modeling identifies distinct dynamic RNA regulatory strategies. *Cell* 159: 1698–1710

Roundtree IA, Luo GZ, Zhang Z, Wang X, Zhou T, Cui Y, Sha J, Huang X, Guerrero L, Xie P *et al* (2017) YTHDC1 mediates nuclear export of N(6)-methyladenosine methylated mRNAs. *eLife* 6: e31311

Samaan Z, Anand SS, Zhang X, Desai D, Rivera M, Pare G, Thabane L, Xie C, Gerstein H, Engert JC *et al* (2013) The protective effect of the obesity-associated rs9939609 a variant in fat mass- and obesity-associated gene on depression. *Mol Psychiatry* 18: 1281–1286

Scuteri A, Sanna S, Chen WM, Uda M, Albai G, Strait J, Najjar S, Nagaraja R, Orru M, Usala G *et al* (2007) Genome-wide association scan shows genetic variants in the FTO gene are associated with obesity-related traits. *PLoS Genet* 3: e115

Shulman Z, Stern-Ginossar N (2020) The RNA modification N(6)-methyladenosine as a novel regulator of the immune system. *Nat Immunol* 21: 501–512

Smemo S, Tena JJ, Kim KH, Gamazon ER, Sakabe NJ, Gomez-Marin C, Aneas I, Credidio FL, Sobreira DR, Wasserman NF *et al* (2014) Obesity-associated variants within FTO form long-range functional connections with IRX3. *Nature* 507: 371–375

Song H, Song J, Cheng M, Zheng M, Wang T, Tian S, Flavell RA, Zhu S, Li HB, Ding C *et al* (2021) METTL3-mediated m(6)a RNA methylation promotes the anti-tumour immunity of natural killer cells. *Nat Commun* 12: 5522

Su R, Dong L, Li Y, Gao M, Han L, Wunderlich M, Deng X, Li H, Huang Y, Gao L *et al* (2020) Targeting FTO suppresses cancer stem cell maintenance and immune evasion. *Cancer Cell* 38: 79–96

Tani H, Akimitsu N (2012) Genome-wide technology for determining RNA stability in mammalian cells: historical perspective and recent advantages based on modified nucleotide labeling. *RNA Biol* 9: 1233–1238

Tong J, Cao G, Zhang T, Sefik E, Amezcua Vesely MC, Broughton JP, Zhu S, Li H, Li B, Chen L *et al* (2018) M(6)a mRNA methylation sustains Treg suppressive functions. *Cell Res* 28: 253–256

Tong J, Wang X, Liu Y, Ren X, Wang A, Chen Z, Yao J, Mao K, Liu T, Meng FL *et al* (2021) Pooled CRISPR screening identifies m(6)a as a positive regulator of macrophage activation. *Sci Adv* 7: eabd4742

Van der Meide PH, Schellekens H (1996) Cytokines and the immune response. *Biotherapy* 8: 243–249

Vivier E, Tomasello E, Baratin M, Walzer T, Ugolini S (2008) Functions of natural killer cells. *Nat Immunol* 9: 503–510

Walters BJ, Mercaldo V, Gillon CJ, Yip M, Neve RL, Boyce FM, Frankland PW, Josselyn SA (2017) The role of the RNA demethylase FTO (fat mass and obesity-associated) and mRNA methylation in hippocampal memory formation. *Neuropsychopharmacology* 42: 1502–1510

Wang X, Lu Z, Gomez A, Hon GC, Yue Y, Han D, Fu Y, Parisien M, Dai Q, Jia G *et al* (2014) N6-methyladenosine-dependent regulation of messenger RNA stability. *Nature* 505: 117–120

Wang X, Zhao BS, Roundtree IA, Lu Z, Han D, Ma H, Weng X, Chen K, Shi H, He C (2015) N(6)-methyladenosine modulates messenger RNA translation efficiency. *Cell* 161: 1388–1399

Wang H, Hu X, Huang M, Liu J, Gu Y, Ma L, Zhou Q, Cao X (2019) Mettl3-mediated mRNA m(6)a methylation promotes dendritic cell activation. *Nat Commun* 10: 1898

Xiang Y, Laurent B, Hsu CH, Nachtergaele S, Lu Z, Sheng W, Xu C, Chen H, Ouyang J, Wang S *et al* (2017) Corrigendum: RNA m(6)a methylation regulates the ultraviolet-induced DNA damage response. *Nature* 552: 430

Xiao W, Adhikari S, Dahal U, Chen YS, Hao YJ, Sun BF, Sun HY, Li A, Ping XL, Lai WY *et al* (2016) Nuclear m(6)a reader YTHDC1 regulates mRNA splicing. *Mol Cell* 61: 507–519

Yang Y, Shen S, Cai Y, Zeng K, Liu K, Li S, Zeng L, Chen L, Tang J, Hu Z *et al* (2021) Dynamic patterns of N6-Methyladenosine profiles of messenger RNA correlated with the cardiomyocyte Regenerability during the early heart development in mice. *Oxid Med Cell Longev* 2021: 5537804

Yin R, Chang J, Li Y, Gao Z, Qiu Q, Wang Q, Han G, Chai J, Feng M, Wang P *et al* (2022) Differential m(6)a RNA landscapes across hematopoiesis reveal a role for IGF2BP2 in preserving hematopoietic stem cell function. *Cell Stem Cell* 29: 149–159

Yu R, Li Q, Feng Z, Cai L, Xu Q (2019) m6A reader YTHDF2 regulates LPS-induced inflammatory response. *Int J Mol Sci* 20: 1323

Zhang C, Zhi WI, Lu H, Samanta D, Chen I, Gabrielson E, Semenza GL (2016) Hypoxia-inducible factors regulate pluripotency factor expression by ZNF217- and ALKBH5-mediated modulation of RNA methylation in breast cancer cells. *Oncotarget* 7: 64527–64542

Zhang C, Chen Y, Sun B, Wang L, Yang Y, Ma D, Lv J, Heng J, Ding Y, Xue Y *et al* (2017) M(6)a modulates haematopoietic stem and progenitor cell specification. *Nature* 549: 273–276

Zhang H, Shi X, Huang T, Zhao X, Chen W, Gu N, Zhang R (2020) Dynamic landscape and evolution of m6A methylation in human. *Nucleic Acids Res* 48: 6251–6264

Zhao X, Yang Y, Sun BF, Shi Y, Yang X, Xiao W, Hao YJ, Ping XL, Chen YS, Wang WJ *et al* (2014) FTO-dependent demethylation of N6-methyladenosine regulates mRNA splicing and is required for adipogenesis. *Cell Res* 24: 1403–1419

Zheng Z, Zhang L, Cui XL, Yu X, Hsu PJ, Lyu R, Tan H, Mandal M, Zhang M, Sun HL *et al* (2020) Control of early B cell development by the RNA N(6)-Methyladenosine methylation. *Cell Rep* 31: 107819

Zhou J, Wan J, Gao X, Zhang X, Jaffrey SR, Qian SB (2015) Dynamic m(6)a mRNA methylation directs translational control of heat shock response. *Nature* 526: 591–594

Zhou J, Zhang X, Hu J, Qu R, Yu Z, Xu H, Chen H, Yan L, Ding C, Zou Q *et al* (2021) M(6)a demethylase ALKBH5 controls CD4(+) T cell pathogenicity and promotes autoimmunity. *Sci Adv* 7: eabg0470

Zhu Y, Zhao Y, Zou L, Zhang D, Aki D, Liu YC (2019) The E3 ligase VHL promotes follicular helper T cell differentiation via glycolytic-epigenetic control. *J Exp Med* 216: 1664–1681

© 2023 The Authors

14693178, 0, Downloaded from https://www.embopress.org/doi/10.15252/embr.202255681 by Korea Research Institute Of, Wiley Online Library on [06/03/2023]. See the Terms and Conditions (https://onlinelibrary.wiley.com/terms-and-conditions) on Wiley Online Library for rules of use; OA articles are governed by the applicable Creative Commons License